A comparison between alkali-activated slag/fly ash binders prepared with natural seawater and deionized water

Ren, Jie; Sun, Hongfang; Li, Qun; Li, Zhenming; Zhang, Xiaogang; Wang, Yanshuai; Li, Linfei; Xing, Feng

DOI
10.1111/jace.18515

Publication date
2022

Document Version
Final published version

Published in
Journal of the American Ceramic Society

Citation (APA)
Ren, J., Sun, H., Li, Q., Li, Z., Zhang, X., Wang, Y., Li, L., & Xing, F. (2022). A comparison between alkali-activated slag/fly ash binders prepared with natural seawater and deionized water. *Journal of the American Ceramic Society*, *105*(9), 5929-5943. https://doi.org/10.1111/jace.18515

Received: 26 November 2021 | Revised: 21 February 2022 | Accepted: 4 April 2022

DOI: 10.1111/jace.18515

Journal of the American Ceramic Society

RESEARCH ARTICLE

A comparison between alkali-activated slag/fly ash binders prepared with natural seawater and deionized water

Jie Ren[1,2] | **Hongfang Sun**[1] | **Qun Li**[1] | **Zhenming Li**[3] | **Xiaogang Zhang**[1] | **Yanshuai Wang**[1] | **Linfei Li**[2] | **Feng Xing**[1]

[1]Guangdong Provincial Key Laboratory of Durability for Marine Civil Engineering, College of Civil and Transportation Engineering, Shenzhen University, Shenzhen, China

[2]Department of Civil, Environment, and Architectural Engineering, University of Colorado Boulder, Boulder, Colorado, USA

[3]Department of Materials and Environment (Microlab), Faculty of Civil Engineering and Geoscience, Delft University of Technology, Delft, The Netherlands

Correspondence
Zhenming Li, Department of Materials and Environment (Microlab), Faculty of Civil Engineering and Geoscience, Delft University of Technology, Delft, The Netherlands.
Email: z.li-2@tudelft.nl

Feng Xing, Guangdong Provincial Key Laboratory of Durability for Marine Civil Engineering, College of Civil and Transportation Engineering, Shenzhen University, Shenzhen 518060, China.
Email: xingf@szu.edu.cn

Funding information
the National Natural Science Foundation of China, Grant/Award Numbers: 51878412, 51520105012, 51878413; the Shenzhen R&D Fund, Grant/Award Number: JCYJ20190808112019066; the Guangdong Provincial Key Laboratory of Durability for Marine Civil Engineering (SZU), Grant/Award Number: 2020B1212060074; the Instrumental Analysis Center of Shenzhen University; National Natural Science Foundation of China, Grant/Award Numbers: 51520105012, 51878412, 51878413

Abstract

In this research, the effects of natural seawater (SW) on the properties of alkali-activated slag/fly ash (AASF) are studied. AASF prepared with deionized water is set as the reference mixture. The results showed that the use of natural SW resulted in a prolonged setting time and lower heat release, but no obvious impact on the flowability of AASF specimens. The long-term compressive strength became higher when SW was used, whereas the corresponding flexural strength and fractural toughness turned lower. The use of SW induced the formation of new products that were not identified in the reference mixture, such as Cl–hydrocalumite and gypsum. In addition, it is evidenced that the dissolution of fly ash (FA) particles was significantly delayed with the incorporation of SW. All these results were related to the various ions introduced by the natural SW and their interactions with the alkaline activator as well as the precipitation of salts on slag and FA surfaces or in the matrix.

KEYWORDS
alkali-activated slag/fly ash, hydration kinetics, mechanical properties, microstructure, seawater, setting time

1 | INTRODUCTION

With the rapid exploitation of coastal and marine resources, there is an increasing demand for building

materials for infrastructures on islands and coastal regions.[1–3] However, traditional ordinary Portland cement (OPC) and freshwater that is required for mixing are not usually available in these areas and long-distance transportation from inland is normally needed. A great deal of manpower and financial cost is hence associated. In fact, even without the concern about transportation cost, freshwater itself is a valuable resource. The production of concrete consumes over 2 billion tons of freshwater every year,[4] accounting for 9% of the overall industrial water usage globally.[5] Scarce freshwater in mainland areas and negative environmental impacts of desalination make the seawater (SW) usage for concrete production imperative.[6] The utilization of SW as a local resource of islands and coastal regions seems to be a reasonable choice for mixing of concrete, because it not only reduces the cost associated with the transportation of freshwater and saves freshwater but also benefits the construction efficiency so as to advance the project schedules.

Many studies have investigated the effect of SW on OPC-based binding materials.[7–12] It is found that SW has a significant impact on the workability and initial setting time of blended OPC/slag concrete.[7] Besides, the 7-day compressive and tensile strength was improved, which is consistent with the higher heat flow compared to that of the freshwater-prepared concrete. However, after 28 days, both the compressive and tensile strengths of the mixture with SW were lower compared to Ref. [7]. It seems that the effects of SW are complicated and require systematic experimental study to elaborate them even for conventional cementitious materials.

Alkali-activated materials (AAMs) have been considered promising alternatives to traditional OPC-based cementitious binders, not only because of the much lower carbon footprint of AAMs,[13–15] but also their comparable or even superior mechanical properties[16–20] and durability against aggressive chemicals, such as sulfate, chloride, and acid.[21–24] Besides, it is worth noting that AAMs do not require a water-curing condition, which is another advantage over OPC-based binders. AAMs are produced by reactions between an alkali metal source (activator) and aluminosilicate solid powders (precursor). For precursors, the most common ones are fly ash (FA), blast furnace slag, and metakaolin,[25–29] depending on local resources and industrial systems of different regions. All these precursors are industrial by-products or natural resources without the need for manufacturing clinkers like in OPC production. For the activator, the most used components are sodium-based hydroxides and silicates,[30] the latter of which are less alkaline.

Among all types of AAMs, alkali-activated slag/fly ash (AASF)-blended binders are gaining increasing attention because of their unique advantages over single-source-based systems, such as reasonable setting time and higher durability in acidic environments.[31–36] However, related literature regarding the effect of SW on AASF binders is quite limited.[37] According to the study,[37] SW and coral sand instead of freshwater and river sand led to a lower drying shrinkage of AASF binders. Besides, the presence of SW and coral sand or sea sand accelerated the formation of C–S–H gels. However, when both fresh water and river sand are substituted by the corresponding SW and sea sand, it is difficult to differentiate the specific effects caused by SW or sea sand. In a recent study,[38] alkali-activated slag (AAS) system prepared with natural SW was studied, but the possible variations in the chemistry and microstructure induced by the incorporation of FA were not known.

In this research, the effects of natural SW on the setting time, flowability, and hydration kinetics of AASF binder (slag/FA = 1:1) were investigated. Besides, mechanical and pore-related properties, as well as mineralogical and microstructural characterization of AASF prepared with SW, were also analyzed. Deionized water (DW)-based AASF counterpart was also synthesized for comparison purposes. Related mechanisms are proposed to explain the properties of AASF materials.

2 | MATERIALS AND METHODS

2.1 | Materials

In this study, the precursor materials, including the ground-granulated blast-furnace slag (GGBFS) and Class F FA, were all supplied by Wuhan SinoCem Smartec Co., Ltd. The GGBFS had a specific gravity of 2900 kg/m^3 with the median particle size (d_{50}) at 12.5 μm. For the FA powders, the specific gravity was 2170 kg/m^3 and the d_{50} was 12.8 μm. The chemical compositions along with the reactive content of silica and alumina of the GGBFS and FA determined by X-ray fluorescence and acid–alkali dissolution according to NEN-EN 196-2 are shown in Table 1, and their X-ray diffraction (XRD) patterns are presented in Figure 1. The particle size distributions of the two precursors are illustrated in Figure 2, and their morphology is shown in Figure 3. Compared to GGBFS with a large amount of constituents as amorphous phases, FA contained many crystalline phases such as mullite, quartz, and hematite, as shown in Figure 1. As shown in Figure 3, GGBFS particles were mainly of irregular shapes, whereas FA had spherical shapes, indicating that the latter would be beneficial for the workability during mixing.

The fine aggregate used in this study to prepare mortar specimens was provided by Xiamen ISO Standard Sand Co., Ltd., in accordance with EN196-1. The natural SW with a density of 1.03 g/cm^3 was obtained at Mawan

TABLE 1 Chemical composition of the GGBFS and FA determined by XRF (wt.%)

Materials	Chemical composition (wt.%)										
	SiO_2/reactive content	CaO	Al_2O_3/reactive content	Fe_2O_3	Na_2O	K_2O	MgO	TiO_2	MnO	SO_3	LOI
GGBFS	29.73/28.91	36.39	13.58/10.09	1.01	0.28	0.55	6.56	0.60	0.09	0.06	0.10
FA	52.45/19.77	6.69	29.35/12.44	5.93	0.89	1.07	0.83	1.24	0.03	0.74	2.41

Abbreviations: FA, fly ash; GGBFS, ground-granulated blast-furnace slag; XRF, X-ray fluorescence.

TABLE 2 The chemical composition of natural seawater used for mixing (g/L)

Ions	Na^+	K^+	Ca^{2+}	Mg^{2+}	Cl^-	SO_4^{2-}	Br^-	F^-	HCO_3^-	BO_3^{3-}
Content	6.67	0.39	0.4	1.2	14.56	1.92	≪0.1	≪0.1	≪0.1	≪0.1

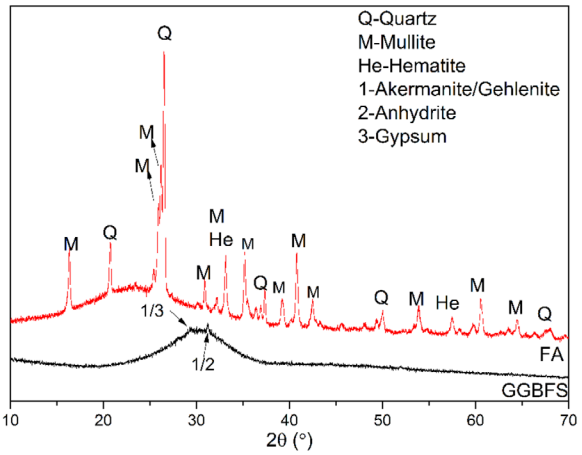

FIGURE 1 X-ray diffraction patterns of the GGBFS and FA with identifications of main phases. FA, fly ash; GGBFS, ground-granulated blast-furnace slag

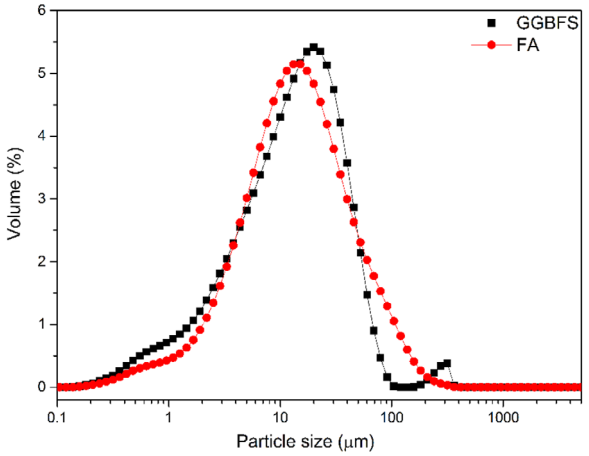

FIGURE 2 Particle size distribution of the GGBFS and FA. FA, fly ash; GGBFS, ground-granulated blast-furnace slag

(113.85°E, 22.51°N) in Qianhai district of Shenzhen, China. The chemical composition of the SW determined by inductively coupled plasma mass spectrometry and ion chromatography is presented in Table 2. It can be seen that Na^+ and Cl^- ions are the most abundant ion species. The pH value of the SW used was 7.61, slightly higher than that (7.03) of the DW. The reason for selecting

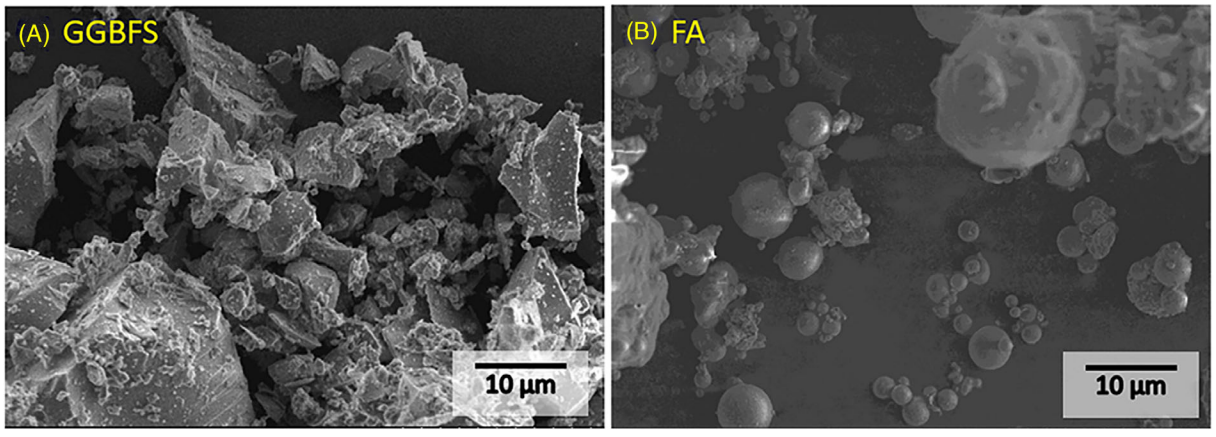

FIGURE 3 SEM images of the GGBFS (A) and FA (B). FA, fly ash; GGBFS, ground-granulated blast-furnace slag. SEM, scanning electron microscopy

TABLE 3 Mixture proportions of the two AASF mortar specimens mixed by SW or DW

Sample ID	Binder (GGBFS:FA)	Mixing water/binder	Anhydrous sodium metasilicate powders (%)	Sand/binder
SW-mortar	50:50	0.38 (SW)	8	2:1
DW-mortar	50:50	0.38 (DW)	8	2:1

For paste specimens, there was no sand added and other parameters were the same as the mortar specimens. Binder refers to the combination of GGBFS and FA.
Abbreviations: AASF, alkali-activated slag/fly ash; DW, deionized water; FA, fly ash; GGBFS, ground-granulated blast-furnace slag; SW, seawater.

natural SW instead of manually synthesized SW was to mimic the real construction circumstances. Anhydrous sodium metasilicate powders (a molar ratio of Si/Na at 1:2) purchased online from Aladdin were mixed with the SW or DW to form the corresponding alkaline activator.

2.2 | Methods

2.2.1 | Sample preparation

In this study, fresh paste specimens were prepared for the determination of the setting time and mineralogical and microstructural characterization. The paste specimens had a water/binder ratio of 0.38. Mortar specimens with the same water/binder ratio and a sand/binder ratio of 2:1 were prepared in order to measure the mechanical and pore-related properties. Prior to mixing, a certain amount of sodium metasilicate powder (8 wt.% of the binder) was first mixed with the natural SW or DW in a beaker until a homogeneous solution was obtained. Following that, the activator solution was allowed to cool down naturally until room temperature (23 ± 2°C) with a plastic film covering the beaker to avoid water evaporation. The pH values of alkaline activator solutions prepared with the SW and DW were measured using a digital pH meter, which were 11.99 and 12.37, respectively. This difference can be explained by considering the interaction between Mg^{2+} from the SW and $Na_2O{\cdot}SiO_2$, which has been detailed in another study.[38] After that, the premixed alkaline activator was added into the dry mixture of GGBFS and FA (for paste) as well as sand (for mortar), which was already mixed for 2 min in a Hobart mixer. The whole mixture was then further mixed for 8 min at low speed before casting into molds with different shapes or directly being used for flowability or setting time measurements. Fresh specimens in molds were vibrated on a vibrating table for about 20 s in order to remove air bubbles. Finally, these specimens were wrapped with cling films tightly to avoid moisture loss for 1 day and then demolded, sealed in plastic bags, and cured in an ambient environment (23 ± 2°C) till the day of testing. Details of the mix proportions of the two types of AASF specimens prepared with the two types of mixing water are tabulated in Table 3.

2.2.2 | Isothermal calorimetry

The hydration heat evolution of the two AASF mixes was recorded using a TAM Air isothermal calorimeter (TA instruments). For each mixture, about 7 g of binder with the ready-mixed alkaline activator solution (either prepared by using the natural SW or DW) was placed and sealed tightly in an ampoule and mixed with a thin wire for about 20 s prior to being inserted into the calorimeter cell. The heat data was recorded continuously during the first 4 days (96 h in total) of hydration. The data within the first 45 min was discarded because of the unavoidable influence of the sample preparation and loading.

2.2.3 | Setting time and flowability measurements

The initial and final setting time was measured according to the Chinese standard GB/T 1346-2001, similar to ASTM C191-19 using a Vicat needle. The flowability of the mortar specimens was determined by using a flow table, based on the Chinese standard GB/T 2419-2005.

2.2.4 | Compressive and flexural strength test

The compressive and flexural strength test was conducted on mortar specimens sizing 40 × 40 × 160 mm. First, three parallel rectangular specimens for each mortar mix were used for the flexural strength test in three-point loading mode at each curing age. The distance between the two supports was 100 mm and the loading rate was 50 N/s. Later on, the residual split specimens in halves (six in total for each mix) were used for the subsequent compressive strength test with a loading rate of 2.4 kN/s. The final results were expressed as the averaged value of the replicates. Besides, the bulk density of these mortar specimens was determined at ages of 1, 3, 7, 28, 56, and 90 days in accordance with ASTM C138/C138M-17a.[39] The average bulk density of three samples at each curing age is reported.

2.2.5 | Pore-related property measurements

The pore-related properties were quantified by measuring the water absorption and volume of permeable voids (VPV) of the mortar specimens, in accordance with ASTM C642-06[40] after 28 and 56 days of curing.

2.2.6 | X-ray diffraction (XRD) analyses

Paste specimens after corresponding curing durations were first broken into small pieces using a hammer and then grounded into fine powder with an agate mortar. The powder that could pass through a 75-μm sieve (No. 200) was then fully immersed in acetone to stop further hydration. Finally, the powder sample was dried in a vacuum oven at 40°C for several days prior to the analysis. The XRD patterns were recorded over the 2θ range of 10–70° with a Bruker D8 Advance diffractometer using Cu K_α radiation. The operating voltage and current were 40 V and 40 mA, respectively.

2.2.7 | Scanning electron microscopy/energy-dispersive spectroscopy (SEM/EDS)

For scanning electron microscopy (SEM) analysis, small fractured specimens were used to compare different morphologies of the paste samples prepared with the natural SW or DW. Prior to the analysis, samples after corresponding curing ages were dried first in a vacuum oven at 40°C for several days and then sealed tightly in a plastic bag to minimize possible carbonation. The analysis was conducted on an FEI Quanta 250 FEG Environmental Scanning Electron Microscope in secondary electron mode. For each paste sample, 20 points were randomly selected in the region of reaction products for energy-dispersive spectroscopy analysis.

3 | RESULTS AND DISCUSSION

3.1 | Setting time and flowability

The initial and final setting time for the SW-paste was 88 and 240 min, respectively. For the DW-paste, the corresponding value was 70 and 219 min. The natural SW prolonged the hardening process of the AASF binding system, although this effect was not that remarkable. This phenomenon can be first attributed to a lower pH value of the alkaline activator when SW was used as the mixing water (pH = 11.99) compared to the one mixed with DW with a pH value of 12.37. The lower pH led to a lower rate of the dissolution of Si–O–Si(Al) from the precursors. Second, some reaction products such as nano-sized M–S–H gels and SiO_2 gels may form via the interaction between the natural SW and sodium metasilicate powders and can cover the surface of GGBFS and FA particles, impeding the dissolution of these particles.[38,41] The prolonged setting time is beneficial for construction fieldwork where a longer operation time is normally required.

In another study,[38] the initial and final setting time for the DW mixed AAS paste was 58 and 88 min, respectively. The addition of FA with a much lower reactivity than that of the GGBFS could explain the longer setting time (70 and 219 min for the initial and final setting time, respectively) of the paste. Interestingly, however, the corresponding value of the same natural SW mixed AAS paste was 123 and 238 min, implying that the 50% replacement of GGBFS by FA led to an earlier initial setting time (88 min), although the opposite seems to be more convincing. This can be associated with the higher amount of solid activator dosage, 8 wt.% used in this study compared to that of 7 wt.% used in Ref. [35] and less water used (the water/binder ratio at 0.38 compared to 0.40), which led to the quicker setting of GGBFS in the GGBFS/FA system compared to the GGBFS alone in the AAS paste. In general, it seems that when the SW was used for mixing, the effect of lower reactivity of FA on the overall mixture diminished. The addition of SW seems to downplay the presence of FA.

The flowability suggested by the spread diameter of the AASF mortar mixed either by SW or DW is shown in Figure 4, which is 168 and 163 mm, respectively. The natural SW mixing slightly improved the flowability of AASF mortar. This result implies that the viscosity of the alkaline activator prepared with the natural SW had a marginal difference compared to the DW prepared alkaline activator. Besides, this also indicates that the effect of different ions in the natural SW on the very early-stage reaction process is insignificant, which could be due to the relatively low concentrations of various ions in the natural SW. The similar flowabilities of the SW mixed and DW mixed alkali-activated binders were also observed in another study.[38] The similar or even improved flowability of the SW mixed AASF mortar suggests a potential of the mixture be used for 3D-printing concrete technologies. Moreover, compared to the pure AAS-based mortar counterpart, which had a flowability of 233 and 235 mm for the SW and DW mixed specimen,[38] the flowability of the AASF mortar sample in this study is smaller. This difference

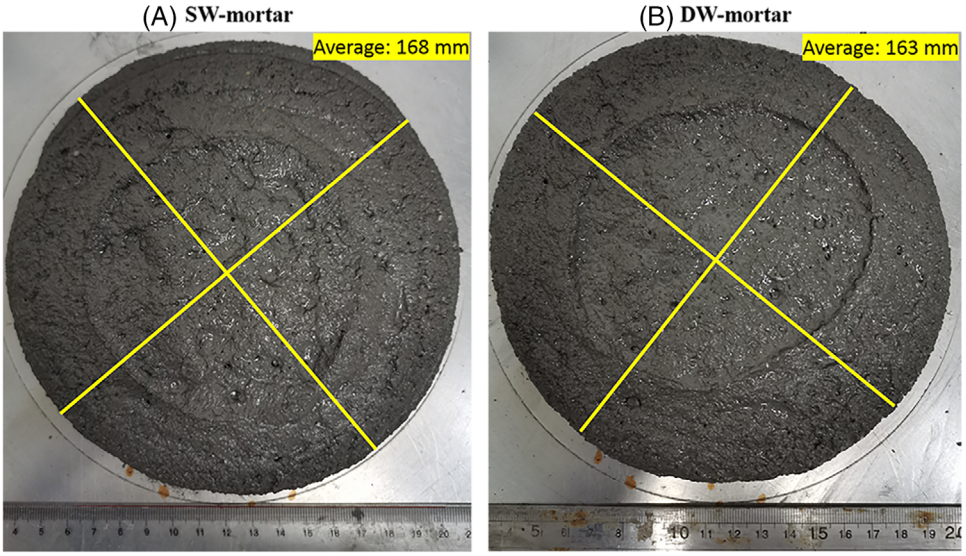

FIGURE 4 Flowability of the fresh AASF mortar, made from (A) SW and (B) DW. The flowability is expressed as the average of the two spreads perpendicular to each other, as marked by yellow lines. AASF, alkali-activated slag/fly ash; DW, deionized water; SW, seawater

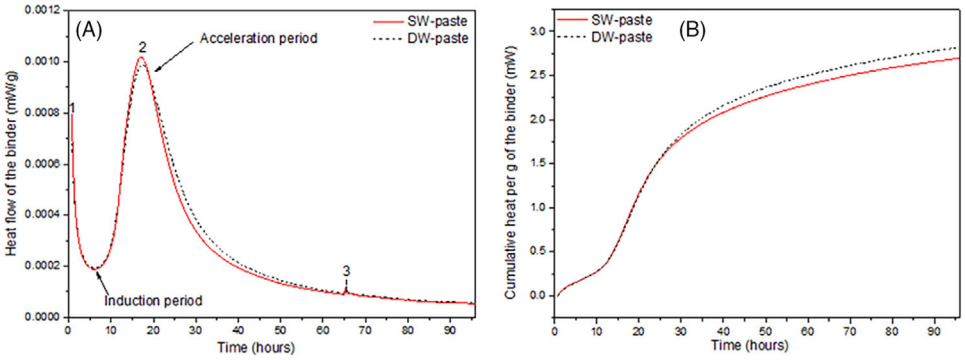

FIGURE 5 (A) Heat flow and (B) cumulative heat (per gram of binder) of SW and DW paste slurries. DW, deionized water; SW, seawater

can be attributed to different amounts of mixing water used while making the mortar specimens as a smaller amount of water could lead to a poorer flowability even though FA in this study could to some extent improve the workability.

3.2 | Reaction kinetics

The heat evolution curves of the two AASF paste mixes within the early reaction process are displayed in Figure 5. Several peaks due to heat release are marked as "1," "2," and "3" from the beginning of the chemical reactions in Figure 5A. The first peak (an initial rising portion) shown as "1" occurred within 1 h after the mixing of the alkaline activator and the combined GGBFS and FA, resulting from the wetting and dissolution of GGBFS and FA particles as well as the adsorption of some ions onto their surfaces.[42–44] In addition, the formation of C–S–H gels due to the presence of Ca^{2+} from both GGBFS and FA or SW and readily available $[SiO_4]^{4-}$ from the alkaline activator could also lead to some heat release in the very early age.[17] The second peak, marked as "2," stretching from 12 to 36 h, is associated with the acceleration period of the reaction.[43,45] Between the peaks "1" and "2," there is an induction period (also known as a dormant period) that can be explained by the following reasons. The first one is that a certain period of time is required before certain ionic species in solution reach a critical concentration for the formation of main reaction products. The second one is the possible coating effect because of the precipitation of C–S–H gels on GGBFS and FA particle surfaces.

Based on the similar intensity of the peak "1," it can be seen that SW has almost no impact on the wetting and dissolution process of precursor, including GGBFS and FA. However, the slightly higher peak "2" for the SW-

paste suggests that SW could, to some extent, promote the acceleration stage of the reaction. This promoted acceleration peak is possibly due to the presence of $CaCl_2$ and sodium chloride (NaCl) with a low concentration in the interstitial solution, in-line with the results from other literature.[46–48] However, it seems that DW-paste exhibited a slightly broader acceleration peak, indicating a better activation, compared to SW-paste.[43] It is noticed that there is a small peak denoted as "3" located after about 65 h from the beginning of the reaction, which might be related to the exposure and reaction of some unreacted precursors, such as FA.

According to Figure 5B, in general, the natural SW seemed to lead to a delayed reaction process, evidenced by the lower cumulative heat release. Hence, it can be concluded that the natural SW slightly facilitated the acceleration reaction but led to a lower cumulative heat release after 4 days of reaction. Comparing the heat flows of the AASF here with that for AAS in Ref. [38], the former of which was significantly lower than the latter. We found that the addition of FA significantly reduced the peak intensity. This is interesting, especially considering the higher alkaline activator dosage (8% of the total binder) and less water usage (water/binder = 0.38) of the former, expectedly leading to a higher alkali concentration and reaction degree and thus a larger amount of heat released during the reaction. This result corresponds well to the findings reported by Rafeet et al.[49] and Li et al.,[50] which showed that FA replacing a partial of slag had a significant impact on the overall reaction process. The result also implies that the AASF-binding system is more suitable for large-volume concrete manufacturing due to its much lower heat release compared to a single slag-based system.

3.3 | Mechanical properties

Figures 6 and 7 show the compressive strength and bulk density of the AASF mortar specimens mixed by using SW or DW during 90 days of curing, respectively. According to Figure 6, it can be seen that there is no significant difference in the compressive strength for the two mortar specimens within 56 days of curing, and there is no obvious pattern to conclude the better one gaining higher compressive strength. For instance, after 7 days, higher compressive strength is seen for the DW-mortar specimens, which was 45.7 MPa, higher than that of the SW mixed specimen, 42.0 MPa. In contrast, after 3 days of curing, it seems that the specimens prepared with DW displayed lower compressive strength than that of the peers mixed by using SW, with a compressive strength of 33.3 and 37.1 MPa, respectively. It is worth pointing out, however, that the difference was not large considering the corresponding standard deviations.

It is also noticed that there was little increase in the compressive strength for the DW mixed AASF mortar specimens from 28 to 90 days of curing, increasing from about 61.6 to 63.1 MPa. In comparison, an increase of up to 14.6% was observed for the SW mixed mortars, from 61.6 to 70.6 MPa. This indicates that DW led to an almost complete compressive strength evolution after 28 days, whereas there is still much potential space for the improvement in the compressive strength when SW is used as the mixing water. Indirectly, this outcome suggests that the natural SW seems to reserve the capacity for the compressive strength development. This can be explained by considering the possible formation of M–S–H gels as there

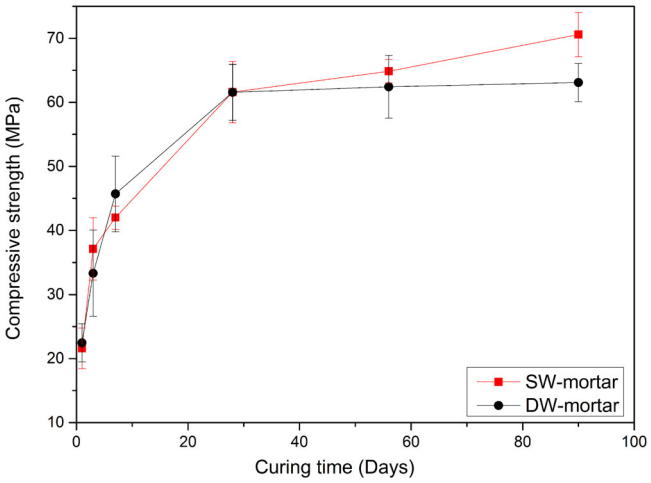

FIGURE 6 Compressive strength of the SW and DW mixed mortar specimens within 90 days of curing. DW, deionized water; SW, seawater

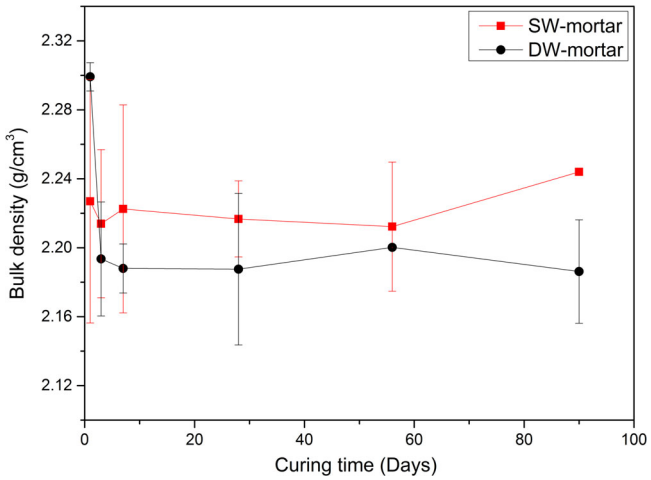

FIGURE 7 Bulk density of the SW and DW mixed mortar specimens within 90 days of curing. DW, deionized water; SW, seawater

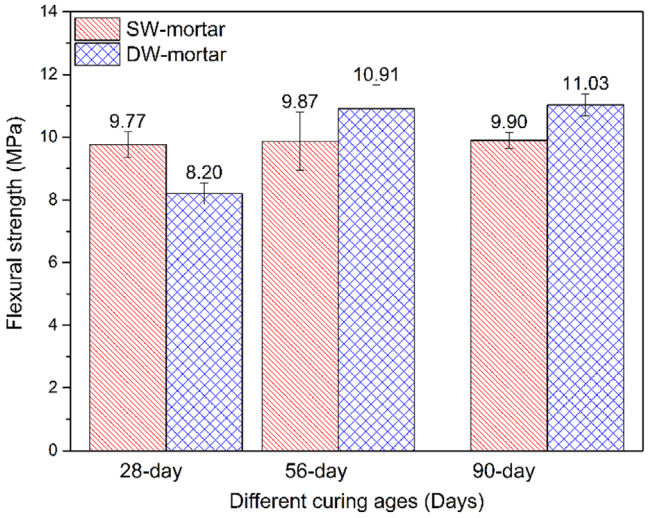

FIGURE 8 Flexural strength of the SW and DW mixed mortar specimens after 28, 56, and 90 days of curing. DW, deionized water; SW, seawater

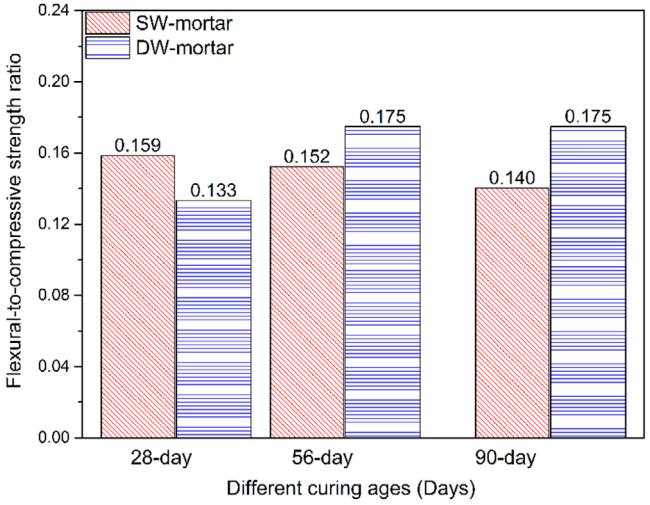

FIGURE 9 Flexural-to-compressive strength ratios of the SW and DW mixed mortar specimens after 28, 56, and 90 days of curing. DW, deionized water; SW, seawater

are available $[SiO_4]^{4-}$ from the prepared alkaline activator and Mg^{2+} ions released from GGBFS particles or in SW, as has been verified by other studies.[38,41] It is highly possible that the M–S–H and SiO_2 gels formed on the surface of GGBFS and FA particles, slowing down the further dissolution of GGBFS and FA particles. As the reaction proceeded, the dissolution of the two precursor materials continued via the loosely formed gels, leading to a later development of the compressive strength. Therefore, SW plays like a retarder in the alkali-activation process of the GGBFS/FA-based binding system. The higher compressive strength after 90 days of curing for the SW-mortar could probably be attributed to precipitations of different salts induced by various ions because of the natural SW mixing, making the microstructure more compact.[51,52]

Based on Figure 7, it is apparent that except at 1 day, SW-mortar had a higher bulk density compared to that of the DW-mortar specimens throughout the 90-day curing period. This is reasonable because the natural SW with a larger density was used in this study (1.03 g/cm^3) than that of the DW (1.0 g/cm^3), which led to an increased amount of each constituent in a unit volume of specimens. As a result, there would be more binding gels and sand per unit volume, leading to a higher bulk density.[47] For the 1-day curing, it is probable that there were fewer hydration products formed, as verified by the longer setting time and lower hydration heat release of the paste specimen. Hence, a lower density was obtained for the SW-mortar.

The flexural strength of the two AASF mixes is presented in Figure 8. After 28, 56, and 90 days of curing, the corresponding flexural strength of the DW-mortar specimens as the reference was 8.2, 10.9, and 11.0 MPa, respectively. For the SW mixed AASF specimens, the corresponding value was 9.8, 9.8, and 9.9 MPa, accordingly. The flexural strength of the SW-mortar was higher than that of the DW prepared counterpart after 28-day curing, representing an increase of 19.1%. However, the natural SW mixing led to a reduced flexural strength by 9.5% and 10.2%, respectively, after 56 and 90 days of curing. The increased flexural strength after 28 days of curing might be attributed to the precipitation of some salts after the evaporation of SW, to some extent bridging the formed hydration products and densifying the microstructure, which is consistent with the result from another study.[37] However, after 56 and 90 days, the decreased flexural strength values might be closely associated with the accumulated pressure from the salt crystallization on the microstructures when there are enough hydration gels but much fewer pores, resulting in a detrimental impact on the final flexural strength. Another possible reason for the reduced flexural strength is the presence of more microcracks in the SW-mortar, as compared to those in the DW-mortar counterpart.[53,54] This hypothesis will be verified in Section 3.6. The inconsistent effects of SW mixing on the flexural strength at different curing ages suggest that it cannot be directly concluded whether SW is beneficial or detrimental to the development of flexural strength.

Based on Figure 9, it can be seen that the flexural-to-compressive strength ratios of the SW mixed mortar specimens declined with the increasing curing ages from 0.16 after 28 days to 0.15 after 56 days and further to 0.14 after 90 days gradually. This is due to a higher rate of compressive strength development compared to that of flexural strength, as evidenced in Figures 6 and 7. In comparison, the flexural-to-compressive strength ratio of the DW mixed mortars increased sharply from 0.13 (28

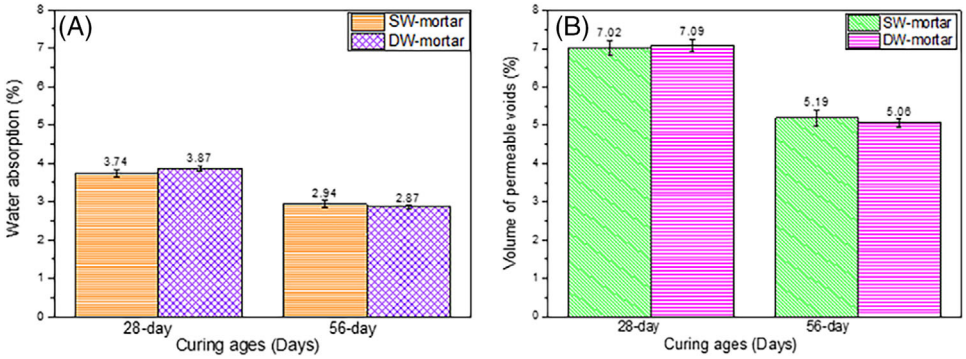

FIGURE 10 (A) Water absorption and (B) VPV of the seawater mixed mortar and deionized water mixed mortar after 28 and 56 days of curing. VPV, volume of permeable voids

days) to 0.18 (56 days) and almost leveled off after 56 days. According to the experimental work conducted by Guo et al.,[55] the flexural-to-compressive strength ratio for the normal OPC mortar after 28 days was 0.17, larger than the value of 0.13 in this study. As the flexural-to-compressive strength ratio is often used as an indicator of toughness for various cementitious binders with a higher value implying a greater toughness,[27,56] the larger value of OPC-based mortar compared to that of the AASF counterpart shows that pure OPC-based binder has a higher toughness than that of the latter. This is in-line with the finding that AASF-based concrete beams have lower initial flexural stiffness compared to that of the conventional OPC-based counterpart.[57] It is worth noting that the flexural-to-compressive strength ratio for the SW-mortar specimens continuously decreases, indicating that SW mixing could be adverse for the long-term performance of AASF binders.

3.4 | Pore-related properties

The water absorption and VPV values of the two AASF mortar mixes after 28 and 56 days of curing are shown in Figure 10. It can be seen that both water absorption and VPV decreased as the curing time increased because of the formation of more hydration products, regardless of the mortar mix. After 28 days of curing, the water absorption and VPV values of SW-mortar specimens were slightly lower than the corresponding values of the mortar prepared using DW. However, the opposite was observed after 56 days of curing. Specifically, the SW mixed mortar specimens had higher water absorption and VPV, 2.9% and 5.2%, respectively, as compared to the corresponding value for the DW prepared mortar, which was accordingly 2.9% and 5.1%. The lower water absorption and VPV correspond well with the slightly higher compressive strength and apparently higher flexural strength of the SW-mortar specimen after 28 days of curing as compared to the DW mixed peer. However, the larger compressive strength of the SW-mortar (64.9 MPa) than that of the DW-mortar counterpart (62.4 MPa) after 56 days seems to contradict the corresponding higher water absorption and VPV values. This can be explained by considering that the slightly larger compressive strength can be neglected especially given the corresponding standard deviations, and the difference between water absorption and VPV values was insignificant in fact. It is worth pointing out that the compressive strength is not only determined by the microstructures of binders, but also dependent on the amount and loading capacities of the binding gels in bulk specimens. On the one hand, there could be more binding gels per unit volume in the SW-mortar as discussed earlier, leading to higher compressive strength. On the other hand, it is possible that after 56 days of curing, the binding gels of the SW-mortar had a higher loading capacity that is probably related to different Ca/Si and Al/Si ratios of the two binding matrices.[58] Further investigations are required to explain this phenomenon. This inconsistent result between water absorption/VPV and compressive strength, specifically higher (lower) values of the former but still higher (lower) values of the latter, has also been reported from previous studies.[38,59,60]

As shown in Figure 11, SW mixed mortar had a larger capillary sorptivity coefficient after 28 days but a lower one after 56 days, compared to the ones of the DW mixed specimens. The inconsistent results from water absorption and VPV and the capillary sorptivity coefficients, which is the higher water absorption and VPV but lower capillary sorptivity coefficients for the DW mixed mortar after 28 days or vice versa for the SW mixed counterpart after 56 days, seem to suggest that these two parameters do not necessarily coincide with each other. Similar results were also obtained from other studies.[38,61] This can be explained by considering that water absorption and VPV reflect the overall porosity, whereas capillary sorptivity mainly indi-

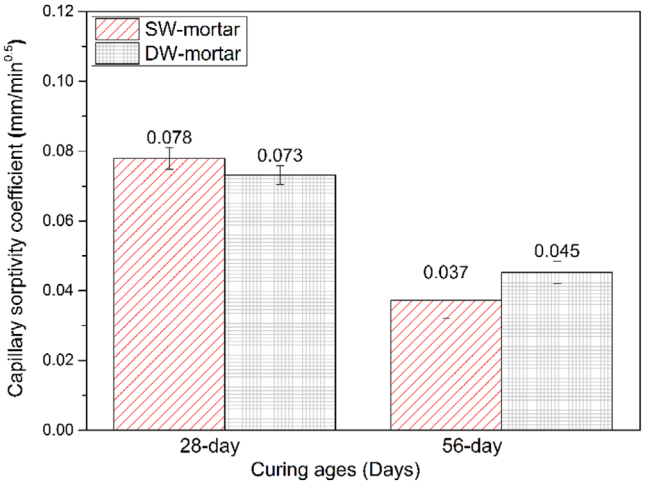

FIGURE 11 Capillary sorptivity coefficients of the seawater and deionized water mixed mortar specimens after 28 and 56 days of curing

cates the volume of capillary pores and related connectivity of porous microstructures.

3.5 | Reaction products

The reaction products of the SW and DW mixed AASF pastes after 3, 28, and 56 days of curing characterized using XRD are shown in Figure 12A,B. The intensity of peaks assigned to the main reaction products C–(N)–(A)–S–H (denoted as "1") and C–A–S–H (denoted as "2") increases gradually as the curing time increases, irrespective of the type of mixing water. For SW-paste, there was a Cl-bearing phase, namely Cl-hydrocalumite (PDF 98-005-1890), which was also identified by Jun et al.[52] For the DW-paste, more peaks associated with the presence of calcite can be observed. In addition, a tiny amount of C–S–H is detected for the DW-paste, which is not detectable in the curves of SW-paste specimens. Gypsum is found in the SW-paste after 28 days of curing, but not after 56 days, which suggests that gypsum is not stable in that binding system or the amount is too small to be tested. All these results indicate that the natural SW used in this study could lead to some changes in the reaction products of the AASF binder with 50% GGBFS and 50% of FA. However, the variations in the final reaction products are not significant, which could be caused by the relatively low concentrations of related ions in this type of SW.

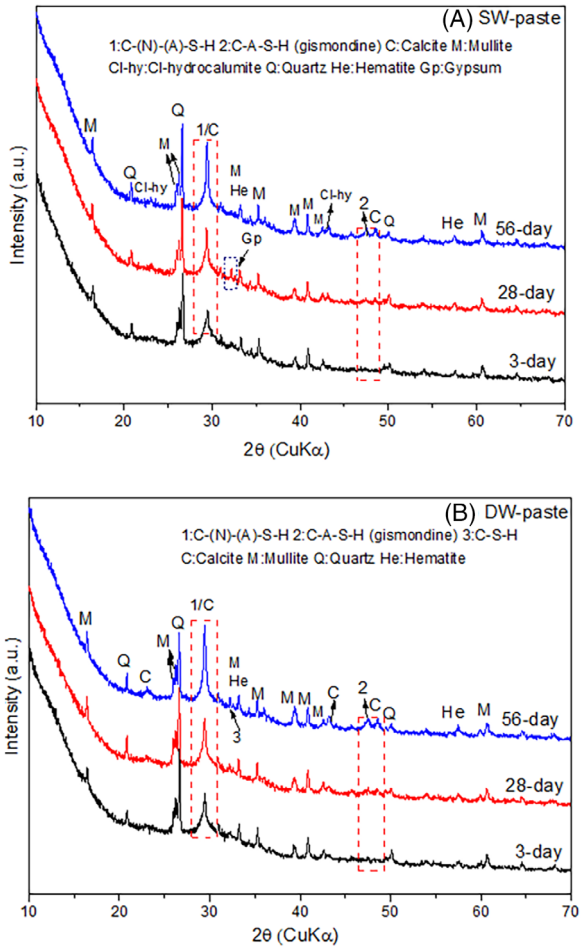

FIGURE 12 XRD patterns of the natural seawater mixed AASF paste (A) and deionized water mixed AASF paste (B) after 3, 28, and 56 days of curing. AASF, alkali-activated slag/fly ash; XRD, X-ray diffraction

3.6 | Morphology and elemental analysis of binders

The morphologies of the two AASF paste mixes after 56 days of curing are shown in Figure 13. It can be seen that both two paste mixes obtained a relatively densified microstructure and smoothed surface either prepared using the natural SW or DW, corresponding well with the similar bulk density of their corresponding mortar specimens after 56 days (see Figure 7).

It is noticed that the residual unreacted FA particles in the SW mixed binding system appear to be much larger in size compared to those in the DW mixed counterpart, as marked by yellow circles. This suggests that the SW -prepared alkaline activator hindered the dissolution and subsequent reactions of FA particles, which is consistent with the lower amount of cumulative heat release during the early stage of the hydration process in Figure 5B. As discussed earlier, the lower pH value and the possible

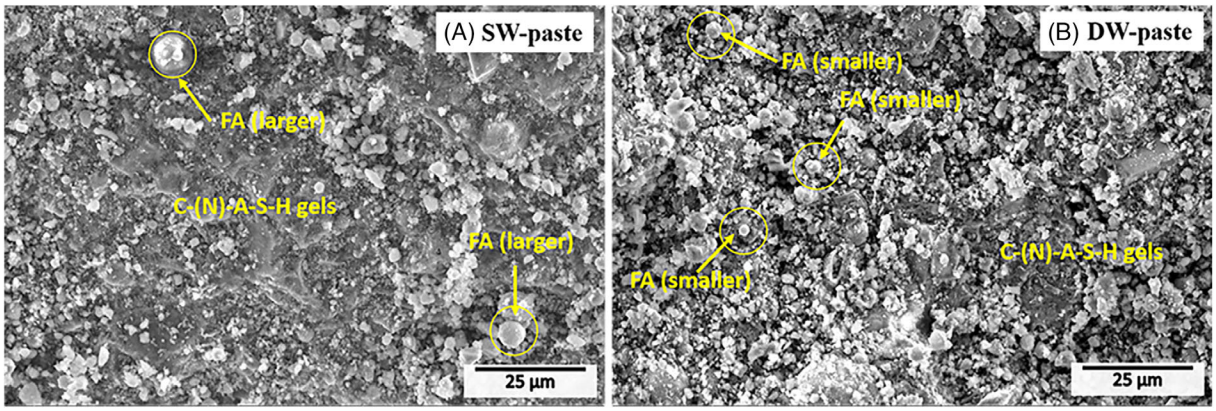

FIGURE 13 Morphologies of the seawater mixed AASF paste (A) and deionized water mixed AASF paste (B) after 56 days of curing based on SEM analysis. AASF, alkali-activated slag/fly ash. SEM, scanning electron microscopy

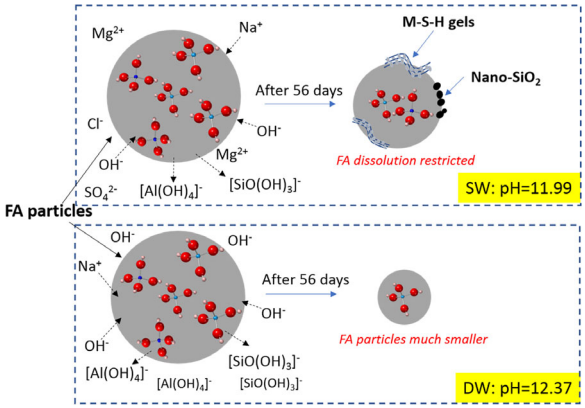

FIGURE 14 Schematic presentation of the delayed dissolution of fly ash in the AASF binding system caused by the seawater mixing. AASF, alkali-activated slag/fly ash

presence of M–S–H and nano-amorphous SiO_2 gels anchoring on the surface of FA particles could explain the lower dissolution rate of FA when the natural SW was used. A schematic presentation of this effect is presented in Figure 14. The insignificant lower cumulative heat release and only 18–21-min difference in the initial and final setting time, but apparently delayed dissolution of FA particles for the SW mixed binder, indicate that FA plays a minor role in the early-stage alkali-activation process (4 days) with the coexistence of GGBFS and FA in a system.

The averaged Ca/Si, Al/Si, and Na/Si atomic ratios for the two binder mixes are shown in Table 4. It can be seen that SW-paste has lower Ca/Si and Al/Si ratios than those of the DW-paste. The much lower Al/Si ratio of SW-paste than that of the DW-paste is consistent with the proposed mechanism depicted in Figure 14 that the dissolution of FA, richer in reactive alumina (12.44%) but with a lower content of reactive silica (19.77%), was to some extent restricted. The higher Ca/Si ratio of the DW-paste is also

TABLE 4 Ca/Si, Al/Si, and Na/Si atomic ratios of the two paste mixes (56 days) based on EDS results. Higher values are highlighted in bold

Sample ID	Ca/Si	Al/Si	Na/Si
SW-paste	1.278	0.407	**0.318**
DW-paste	**1.301**	**0.702**	0.199

Abbreviations: DW, deionized water; EDS, energy dispersive spectroscopy; SW, seawater.

in-line with the additional formation of C–S–H gels found in XRD patterns (Figure 12B). Based on some previous research,[63,64] lower Ca/Si ratios led to increased stiffness, elastic modulus, and hardness of C–S–H gels. Considering the main reaction product should be a silicate structure of C–S–H with Q1 and Q2 units similar to OPC as the content of GGBFS was 50% in the precursor,[65] the lower Ca/Si ratio of SW-paste corresponds well with its slightly higher 56-day compressive strength than that of the DW-paste (Figure 6). Besides, the lower Al/Si (higher Si/Al) of the SW-paste corresponds well with its extended setting time and higher compressive strength as mentioned earlier and the findings from other studies.[66,67] A higher Na/Si ratio, however, is observed in the SW-paste, which should be due to the introduction of sodium ions from the natural SW into the binding matrix. It seems that some sodium salts are embedded in the binding matrix, which has also been reported by the literature.[38] Besides, the relationship between Si/Ca versus Al/Ca ratios of all points that were used for elemental analysis is shown in Figure 15, and the results indicate that the main reaction products of the two binding mixes are C–A–S–H[65] and C–(N)–A–S–H with low Ca content,[66] corresponding well with the XRD results (Figure 12).

The morphologies of the two AASF mortar mixes after 56 days of curing are shown in Figure 16. According to Figure 16, there are some small cracks in the interfacial

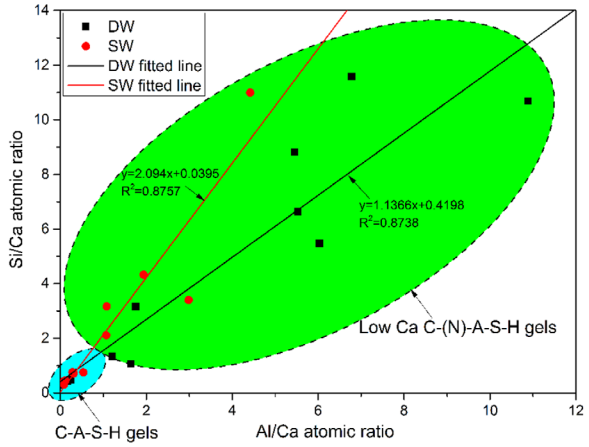

FIGURE 15 Si/Ca ratios versus Al/Ca ratios of the two binding mixes based on the EDS results. EDS, energy dispersive spectroscopy

transition zone (ITZ) between the sand and binding matrix for the SW-mortar, whereas there are almost no such cracks in the ITZ for the DW-mortar specimen. This is in-line with the slightly lower flexural strength of the SW-mortar compared to that of the DW-mortar as flexural strength is highly determined by the bonding between fine aggregate and the binding matrix.

4 | CONCLUSIONS

In this work, the influences of natural SW mixing on the fresh and hardened properties of AASF-based binders are investigated. The following conclusions are presented based on the findings of this research:

- The use of natural SW could slightly facilitate the acceleration stage of the alkali-activation reaction but reduce the overall reaction degree as evidenced by delayed setting time and lower cumulative hydration heat.
- The flexural strength and toughness from 56 days of curing were decreased because of the natural SW, but the corresponding compressive strength after 56 and 90 days of curing showed an increase.
- When SW was used as the mixing water, new hydration products such as Cl-hydrocalumite and gypsum were formed within the binding matrix, and the gel had lower Ca/Si and Al/Si ratios.
- The natural SW had little impact on the flowability of the AASF mortar specimens.
- The obvious delayed dissolution of FA when using SW as evidenced from SEM results but the relatively small difference in the setting time and cumulative heat release between the SW and DW mixed specimens suggest that FA plays a minor role in the alkali-activation process of GGBFS and FA blends when SW was used. The SW seems to weaken the involvement of FA in reactions.

In general, this study confirms that the natural SW used has a strong potential as a replacement of freshwater for the mixing of AASF binders with a slightly improved flowability, prolonged but still acceptable setting time, higher long-term compressive strength, and relatively densified microstructure. One topic for future research is the durability of this SW mixed AASF binder in marine environments such as its resistance to drying-wetting cycles, chloride, and sulfate attacks, which determine the service life of concrete structures made from this type of binder.

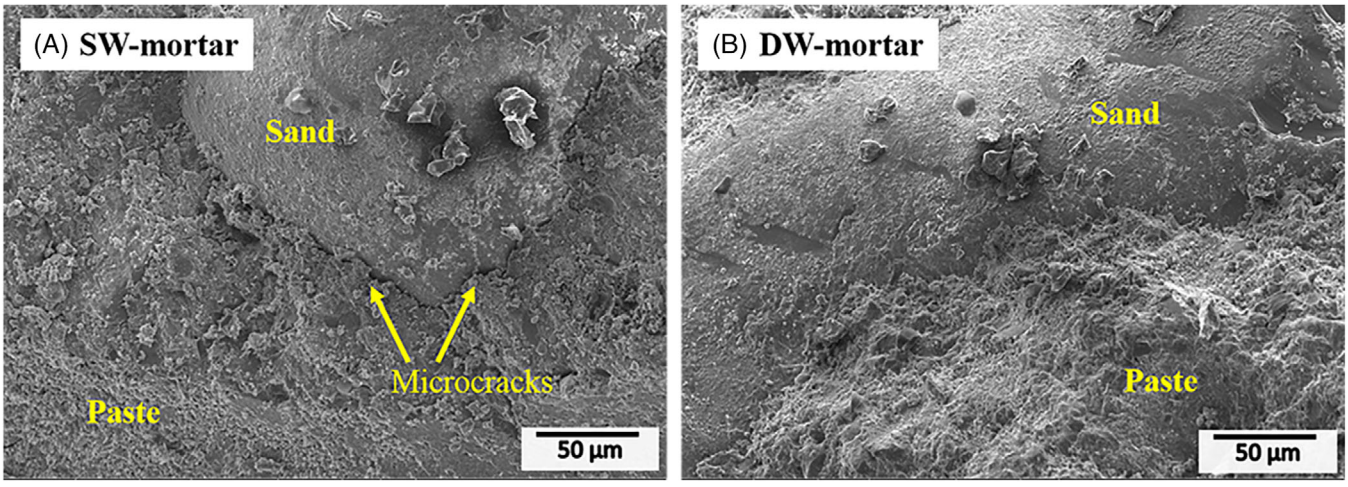

FIGURE 16 Morphologies of the seawater mixed AASF mortar (A) and distilled water mixed AASF mortar (B) after 56 days of curing based on SEM analysis. AASF, alkali-activated slag/fly ash. SEM, scanning electron microscopy

ACKNOWLEDGMENTS

The authors wish to acknowledge the support from the National Natural Science Foundation of China (Grant nos. 51878412, 51520105012, and 51878413), the Shenzhen R&D Fund (Grant no. JCYJ20190808112019066), and the Guangdong Provincial Key Laboratory of Durability for Marine Civil Engineering (SZU) (Grant no. 2020B1212060074). Besides, the Instrumental Analysis Center of Shenzhen University is also acknowledged.

CONFLICT OF INTEREST

None.

REFERENCES

1. Wang Y, Zhang S, Niu D, Su L, Luo D. Effects of silica fume and blast furnace slag on the mechanical properties and chloride ion distribution of coral aggregate concrete. Constr Build Mater. 2019;214:648–58.
2. lyu B, Wang A, Zhang Z, Liu K, Xu H, Shi L, et al. Coral aggregate concrete: numerical description of physical, chemical and morphological properties of coral aggregate. Cem Concr Compos. 2019;100:25–34.
3. Wang Y, Shui Z, Huang Y, Sun T, Duan P. Properties of coral waste-based mortar incorporating metakaolin: Part II. Chloride migration and binding behaviors. Constr Build Mater. 2018;174:433–42.
4. Miller SA, Horvath A, Monteiro PJM. Readily implementable techniques can cut annual CO_2 emissions from the production of concrete by over 20%. Environ Res Lett. 2016;11(7): 074029.
5. Miller SA, Horvath A, Monteiro PJM. Impacts of booming concrete production on water resources worldwide. Nat Sustain. 2018;1(1):69–76.
6. Lee K, Jepson W. Environmental impact of desalination: a systematic review of life cycle assessment. Desalination. 2021;509:115066.
7. Younis A, Ebead U, Suraneni P, Nanni A. Fresh and hardened properties of seawater-mixed concrete. Constr Build Mater. 2018;190:276–86.
8. Wegian FM. Effect of seawater for mixing and curing on structural concrete, IES J A Civil Struct Eng. 2010;3(4):235–43.
9. Cheng S, Shui Z, Sun T, Huang Y, Liu K. Effects of seawater and supplementary cementitious materials on the durability and microstructure of lightweight aggregate concrete. Constr Build Mater. 2018;190:1081–90.
10. Otsuki N, Furuya D, Saito T, Tadokoro Y. Possibility of sea water as mixing water in concrete. In: Conference on Our World in Concrete & Structures, Tokyo Institute of Technology, Japan (2011).
11. Xiao J, Qiang C, Nanni A, Zhang K. Use of sea-sand and seawater in concrete construction: current status and future opportunities. Constr Build Mater. 2017;155:1101–11.
12. Qu F, Li W, Tang Z, Wang K. Property degradation of seawater sea sand cementitious mortar with GGBFS and glass fiber subjected to elevated temperatures. J Mater Res Technol. 2021;13:366–84.
13. Duxson P. Geopolymers, structure, processing, properties and applications, In: Provis,J. Van Deventer, J. (eds.), Woodhead Publishing Limited Abington Hall, Cambridge, UK (2009).
14. Huseien GF, Hamzah HK, Mohd Sam AR, Khalid NHA, Shah KW, Deogrescu DP, et al. Alkali-activated mortars blended with glass bottle waste nano powder: environmental benefit and sustainability, J Cleaner Prod. 2020;243:118636.
15. Huseien GF, Sam ARM, Shah KW, Budiea AMA, Mirza J. Utilizing spend garnets as sand replacement in alkali-activated mortars containing fly ash and GBFS, Constr Build Mater. 2019;225:132–45.
16. Temuujin J, Riessen AV, Williams R. Influence of calcium compounds on the mechanical properties of fly ash geopolymer pastes. J Hazard Mater. 2009;167(1–3):82–8.
17. Brough AR, Atkinson A. Sodium silicate-based, alkali-activated slag mortars: Part I. Strength, hydration and microstructure. Cem Concr Res. 2002;32(6):865–79.
18. Safari Z, Kurda R, Al-Hadad B, Mahmood F, Tapan M. Mechanical characteristics of pumice-based geopolymer paste. Resour Conserv Recycl. 2020;162:105055.
19. Kakria K, Thirumalini S, Secco M, Shanmuga Priya T. A novel approach for the development of sustainable hybridized geopolymer mortar from waste printed circuit boards. Resour Conserv Recycl. 2020;163:105066.
20. Ren J, Guo S-Y, Qiao X-L, Zhao T-J, Zhang L-H, Chen J-C, et al. A novel titania/graphene composite applied in reinforcing microstructural and mechanical properties of alkali-activated slag. J Build Eng. 2021;41:102386.
21. Temuujin J, Minjigmaa A, Lee M, Chen-Tan N, van Riessen A. Characterisation of class F fly ash geopolymer pastes immersed in acid and alkaline solutions. Cem Concr Compos. 2011;33(10):1086–91.
22. Ren J, Zhang L, San Nicolas R. Degradation process of alkali-activated slag/fly ash and Portland cement-based pastes exposed to phosphoric acid. Constr Build Mater. 2020;232:117209.
23. Bernal SA, Rodríguez ED, Mejía de Gutiérrez R, Provis JL. Performance of alkali-activated slag mortars exposed to acids. J Sustain Cem Based Mater. 2012;1(3):138–51.
24. Shi C, Zhang L, Zhang J, Li N, Ou Z. Advances in testing methods and influencing factors of chloride ion transport properties of alkali-activated materials. Mater Rep. 2017;31(15):95–100.
25. Ozer I, Soyer-Uzun S. Relations between the structural characteristics and compressive strength in metakaolin based geopolymers with different molar Si/Al ratios, Ceram Int. 2015;41(8):10192–8.
26. Ren J, Guo S, Su J, Zhao T, Chen J, Zhang S. A novel TiO_2/Epoxy resin composited geopolymer with great durability in wetting-drying and phosphoric acid solution. J Cleaner Prod. 2019;227:849–60.
27. Ren J, Guo S, Zhao T, Chen J, San Nicolas R, Zhang L. Constructing a novel nano-TiO_2/Epoxy resin composite and its application in alkali-activated slag/fly ash pastes. Constr Build Mater. 2020;232:117218.
28. Ye H, Cartwright C, Rajabipour F, Radlińska A. Understanding the drying shrinkage performance of alkali-activated slag mortars. Cem Concr Compos. 2017;76:13–24.
29. Yousefi Oderji S, Chen B, Jaffar STA. Effects of relative humidity on the properties of fly ash-based geopolymers. Constr Build Mater. 2017;153:268–73.

30. Provis JL, Van Deventer JS. Alkali activated materials: state-of-the-art report, RILEM TC 224-AAM, Springer Science & Business Media. 2013. https://books.google.nl/books?hl=zh-CN&lr=&id=fvXHBAAAQBAJ&oi=fnd&pg=PR5&dq=Alkali+activated+materials:+state%E2%80%90of%E2%80%90the%E2%80%90art+report,+RILEM+TC+224%E2%80%90AAM&ots=k5TM-XIwyG&sig=R1TkpX59MpAiu6MVkhHYLHYP7uI&redir_esc=y#v=onepage&q=Alkali%20activated%20materials%3A%20state%E2%80%90of%E2%80%90the%E2%80%90art%20report%2C%20RILEM%20TC%20224%E2%80%90AAM&f=false
31. Liu Y, Zhu W, Yang E-H. Alkali-activated ground granulated blast-furnace slag incorporating incinerator fly ash as a potential binder. Constr Build Mater. 2016;112:1005–12.
32. Puertas F, Fernández-Jiménez A. Mineralogical and microstructural characterisation of alkali-activated fly ash/slag pastes. Cem Concr Compos. 2003;25(3):287–92.
33. Li Z, Liu S. Influence of slag as additive on compressive strength of fly ash-based geopolymer. J Mater Civ Eng. 2007;19(6):470–4.
34. Lloyd RR, Provis JL, Van Deventer JS. Pore solution composition and alkali diffusion in inorganic polymer cement. Cem Concr Res. 2010;40(9):1386–92.
35. Nedeljković M, Li Z, Ye G. Setting, strength, and autogenous shrinkage of alkali-activated fly ash and slag pastes: effect of slag content. Materials. 2018;11(11):2121.
36. Ren J, Zhang L, Zhu Y, Li Z, San Nicolas R. A comparative study on the degradation of alkali-activated slag/fly ash and cement-based mortars in phosphoric acid. Front Mater. 2022;9.
37. Zhang B, Zhu H, Shah KW, Dong Z, Wu J. Performance evaluation and microstructure characterization of seawater and coral/sea sand alkali-activated mortars. Constr Build Mater. 2020;259:120403.
38. Ren J, Sun H, Cao K, Ren Z, Zhou B, Wu W, et al. Effects of natural seawater mixing on the properties of alkali-activated slag binders. Constr Build Mater. 2021;294:123601.
39. American Society for Testing and Materials (ASTM) C138, Standard Test Method for Density (Unit Weight), Yield, and Air Content (Gravimetric). 2001.
40. C. ASTM. 642, Standard test method for density, absorption, and voids in hardened concrete, Annual book of ASTM standards 4. 2006.
41. Shi D, Yao Y, Ye J, Zhang W. Effects of seawater on mechanical properties, mineralogy and microstructure of calcium silicate slag-based alkali-activated materials. Constr Build Mater. 2019;212:569–77.
42. Shi C, Day RL. A calorimetric study of early hydration of alkali-slag cements. Cem Concr Res. 1995;25(6):1333–46.
43. Chithiraputhiran S, Neithalath N. Isothermal reaction kinetics and temperature dependence of alkali activation of slag, fly ash and their blends. Constr Build Mater. 2013;45:233–42.
44. Ravikumar D, Neithalath N. Reaction kinetics in sodium silicate powder and liquid activated slag binders evaluated using isothermal calorimetry. Thermochim Acta. 2012;546:32–43.
45. Nedunuri ASSS, Muhammad S. Fundamental understanding of the setting behaviour of the alkali activated binders based on ground granulated blast furnace slag and fly ash. Constr Build Mater. 2021;291:123243.
46. Lv W, Sun Z, Su Z. Study of seawater mixed one-part alkali activated GGBFS-fly ash. Cem Concr Compos. 2020;106:103484.
47. Yang S, Xu J, Zang C, Li R, Yang Q, Sun S. Mechanical properties of alkali-activated slag concrete mixed by seawater and sea sand. Constr Build Mater. 2019;196:395–410.
48. Brough A, Holloway M, Sykes J, Atkinson A. Sodium silicate-based alkali-activated slag mortars: Part II. The retarding effect of additions of sodium chloride or malic acid. Cem Concr Res. 2000;30(9):1375–9.
49. Rafeet A, Vinai R, Soutsos M, Sha W. Effects of slag substitution on physical and mechanical properties of fly ash-based alkali activated binders (AABs). Cem Concr Res. 2019;122:118–35.
50. Li Z, Lu T, Liang X, Dong H, Ye G. Mechanisms of autogenous shrinkage of alkali-activated slag and fly ash pastes. Cem Concr Res. 2020;135:106107.
51. Rashad AM, Ezzat M. A Preliminary study on the use of magnetic, Zamzam, and sea water as mixing water for alkali-activated slag pastes. Constr Build Mater. 2019;207:672–8.
52. Jun Y, Kim T, Kim JH. Chloride-bearing characteristics of alkali-activated slag mixed with seawater: effect of different salinity levels. Cem Concr Compos. 2020;112:103680.
53. Li Z, Lu T, Chen Y, Wu B, Ye G. Prediction of the autogenous shrinkage and microcracking of alkali-activated slag and fly ash concrete. Cem Concr Compos. 2021;117:103913.
54. Li Z, Nedeljković M, Chen B, Ye G. Mitigating the autogenous shrinkage of alkali-activated slag by metakaolin. Cem Concr Res. 2019;122:30–41.
55. Guo S-Y, Zhang X, Chen J-Z, Mou B, Shang H-S, Wang P, et al. Mechanical and interface bonding properties of epoxy resin reinforced Portland cement repairing mortar. Constr Build Mater. 2020;264:120715.
56. Wang R, Lackner R, Wang PM. Effect of styrene–butadiene rubber latex on mechanical properties of cementitious materials highlighted by means of nanoindentation. Strain. 2011;47(2):117–26.
57. Du Y, Wang J, Shi C, Hwang H-J, Li N. Flexural behavior of alkali-activated slag-based concrete beams. Eng Struct. 2021;229:111644.
58. He P, Wang M, Fu S, Jia D, Yan S, Yuan J, et al. Effects of Si/Al ratio on the structure and properties of metakaolin based geopolymer. Ceram Int. 2016;42(13):14416–22.
59. Ren J, Zhang L, Walkley B, Black JR, San Nicolas R. Degradation resistance of different cementitious materials to phosphoric acid attack at early stage. Cem Concr Res. 2022;151:106606.
60. Ren J, Zhang L, San Nicolas R. Degradation of alkali-activated slag/fly ash mortars under different aggressive acid conditions. J Mater Civil Eng. 2020.
61. Olivia M, Nikraz H. Properties of fly ash geopolymer concrete designed by Taguchi method. Mater Des. 2012;36:191–8.
62. Yubin J, Seyoon Y, Jae O. A comparison study for chloride-binding capacity between alkali-activated fly ash and slag in the use of seawater. Appl Sci. 2017;7(10):971.
63. Pelisser F, Gleize P, Mikowski A. Effect of the Ca/Si molar ratio on the micro/nanomechanical properties of synthetic C–S–H measured by nanoindentation. J Phys Chem C. 2012;116:17219–27.

64. Hou D, Li H, Zhang L, Zhang J. Nano-scale mechanical properties investigation of C–S–H from hydrated tri-calcium silicate by nano-indentation and molecular dynamics simulation. Constr Build Mater. 2018;189:265–75.
65. Lecomte I, Henrist C, Liégeois M, Maseri F, Rulmont A, Cloots R. (Micro)-structural comparison between geopolymers, alkali-activated slag cement and Portland cement. J Eur Ceram Soc. 2006;26(16) :3789–97.
66. Punurai W, Kroehong W, Saptamongkol A, Chindaprasirt P. Mechanical properties, microstructure and drying shrinkage of hybrid fly ash-basalt fiber geopolymer paste. Constr Build Mater. 2018;186:62–70.
67. Zhang M, Zhao M, Zhang G, El-Korchi T, Tao M. A multiscale investigation of reaction kinetics, phase formation, and mechanical properties of metakaolin geopolymers. Cem Concr Compos. 2017;78:21–32.

How to cite this article: Ren J, Sun H, Li Q, Li Z, Zhang X, Wang Y, et al. A comparison between alkali-activated slag/fly ash binders prepared with natural seawater and deionized water. J Am Ceram Soc. 2022;105:5929–5943.
https://doi.org/10.1111/jace.18515